Formation, remobilisation and alteration processes at inactive hydrothermal vents: insights from elemental analysis of Cu-(Fe-)S sulfides from TAG, Mid-Atlantic Ridge

Berit Lehrmann[1*], Matthew J. Cooper[2], J. Andy Milton[2], Bramley J. Murton[1]

[1]National Oceanography Centre, European Way, Southampton SO14 3ZH, UK

[2]School of Ocean and Earth Science, University of Southampton Waterfront Campus, European Way, Southampton, SO14 3ZH, UK

Corresponding author: beleh7@gmx.de,

Abstract

Chalcopyrite is the main Cu mineral in mafic hosted marine hydrothermal systems. Its trace element budget and that of its alteration products may hold valuable information on formation, remobilisation and alteration processes of the hydrothermal system. In this study we analysed chalcopyrite from five inactive seafloor massive sulfide (SMS) sites from the TAG hydrothermal field on the Mid-Atlantic Ridge by electron probe microanalysis (EPMA) and laser ablation inductively coupled plasma mass spectrometry (LA-ICP-MS) for 24 elements. Twelve of them are discussed in detail. In general, trace element concentrations range between sub-parts per million (ppm) to several hundreds of ppm. The elements Se and Co are incorporated into the lattice at high temperatures of >300 °C, whereas As, Ge, Ga substitute into the structure at intermediate to low temperatures. Other elements, e.g. Zn, are either accommodated into the mineral lattice or form inclusions, whereas V and Mn, which originate from seawater, get adsorbed onto the mineral surface. Idaite, chalcocite, and covellite exhibit similar trace element patterns to those of the precursor chalcopyrite. However, the secondary copper minerals show enrichment of Ag and Mo. Factors controlling the incorporation are predominantly related to changes in physicochemical conditions with the host rock composition playing only a minor role.

Key words: TAG hydrothermal field, seafloor massive sulfides, trace elements, LA-ICP-MS

Introduction

SMS deposits formed through hydrothermal venting in today's oceans are considered the modern analogue of ancient volcanogenic massive sulfide deposits (VMS). Based on their tectonic setting SMS can be rich in metals such as copper, zinc and gold (Hannington et al. 2005, Monecke et al. 2016). Currently, there are more than 600 SMS sites known (Beaulieu et al. 2015) containing an estimated global resource of 600 million tonnes of sulfide with a median grade of 9 wt.% Zn, 3 wt.% Cu, 100 g/t Ag and 2 g/t Au (Hannington et al. 2011, Monecke et al. 2016). With the increasing interest

of our society to move towards a sustainable low carbon footprint future with renewable energies and efficient technologies (Mudd et al. 2017), and to decouple metal production from carbon emission (Wang and Feng 2019), the mining industry is looking for alternative metal sources to meet these goals. Although it will be unlikely that SMS are targeted because of their base and precious metal grades (Singer 2014), they might be of interest with regard to their trace metal budget. Previous work on this topic is scarce with Monecke et al. (2016) presenting the most comprehensive study so far. However, they considered only bulk geochemical data, which does not decipher the host mineral for a specific trace element though this is essential information for metal extraction processes (Rankin 2017).

LA-ICP-MS provides high sensitivity, multi element analyses at a spatial resolution of a few micrometres; this utility permits the in depth investigation of trace elements in specific minerals. Pyrite and sphalerite are the predominant minerals investigated from SMS sites with regard to their trace element budget (Melekestseva et al. 2014, Wohlgemuth-Ueberwasser et al. 2015, Keith et al. 2016, Melekestseva et al. 2017, Grant et al. 2018, Maslennikov et al. 2020, Meng et al. 2020). In situ LA-ICP-MS on pyrite and sphalerite has shown that the combination of trace element concentrations of different mineral generations can be used to decipher processes related to precipitation, metal remobilisation and source of the metals (Wohlgemuth-Ueberwasser et al. 2015, Keith et al. 2016, Melekestseva et al. 2017, Grant et al. 2018, Melekestseva et al. 2020). Studies on chalcopyrite, a common phase in mafic and ultramafic hosted SMS sites, are, however limited. Where chalcopyrite was analysed the data only consider a few of elements (Butler and Nesbitt 1999, Wohlgemuth-Ueberwasser et al. 2015, Dekov et al. 2018, Yuan et al. 2018) with limited studies reporting Ga, Ge, Se and In (Wang et al. 2017, Grant et al. 2018). Whilst chalcopyrite is a common copper mineral and is one of the main sources for copper in the mining industry, it was thought that it was a poor host for trace elements (George et al. 2016). However, George et al. (2018) showed this not to be the case.

In this study, in situ LA-ICP-MS trace element composition of chalcopyrite and its secondary alteration phases from five hydrothermally inactive SMS sites from the TAG hydrothermal field are presented and discussed. All SMS sites are hosted in basalt and should exhibit very similar trace element patterns, if the host rock had a significant influence on the trace metal composition (Wohlgemuth-Ueberwasser et al. 2015). However, the trace element composition should vary if the host rock only had a minor role with Keith et al. (2016) proposing that changes of pH, temperature, redox potential and salinity being the key factors influencing the trace element composition of hydrothermal precipitates. Our results show that all Cu-(Fe-)S sulfides can host a wide range of trace elements, ranging in the concentrations from sub-ppm to several hundred ppm, with the majority being incorporated into the mineral lattice.

Geological Setting

The basalt hosted TAG hydrothermal field at 26°09'N is one of the largest and best studied hydrothermal systems on earth (Rona et al. 1986, 1993, Hannington et al. 1998, Tivey et al. 2003, Humphris et al. 2015). Numerous active and relict mound shaped hydrothermal sites are located in an area of 5 km^2 on the eastern side of the axial valley of the Mid-Atlantic Ridge with mounds varying in size, stage of development and age. The active TAG mound, located in the southwest of the area (Fig. 1), is currently in a high temperature venting stage, i.e. metal rich black smoker fluids at ~365 °C are being discharged through multiple chimneys on the so called "upper platform". At the "lower platform" a ~50 °C diffuse flow has been detected (Humphris et al. 2015). The main lithology on the "upper platform" is an anhydrite rich massive sulfide that is partially brecciated and predominantly composed of chalcopyrite and pyrite (Hannington et al. 1991). On the "lower platform" a silica rich massive sulfide predominates and contains sphalerite, marcasite and pyrite. During Ocean Drilling Programme Leg 158, in the mid 1990s, the active TAG mound was drilled to a depth of 125 metre below seafloor (mbsf). Lithologies encountered were massive pyrite breccia, anhydrite rich pyrite breccia, silica rich pyrite breccia and altered wall rock and basalt in the deepest parts of the mound (Humphris et al. 2015, Grant et al. 2018). Only the upper five meters of the mound seem to be enriched in minerals of economic interest, with the remaining mound being composed of barren pyrite (Hannington et al. 1998).

North northeast of the active TAG mound several hydrothermal extinct mounds occur: Southern, Rona, Double, Shinkai, New Mound 2 and New Mound 3 (Fig. 1). Surface samples from Shinkai mound, New Mound 2 and 3 comprise chimney fragments whereas pyrite rich sulfide breccia and massive sulfides were recovered from the surface and subsurface of Southern and Rona mound (Lehrmann et al. 2018, Murton et al. 2019).

Another hydrothermally inactive SMS area of around 1 km^2, the MIR zone, is located 2 km to the north northeast of the active TAG mound (Fig. 1). In comparison to the other mounds, large distinctive surface features (e.g., upright chimneys) are absent in the MIR zone, although White et al. (1998) documented a small mound of 100 m diameter and 10 m height. The main surface rock types comprise chimney fragments and blocks of massive sulfides (Stepanova et al. 1996), though drilling in 2016 revealed the occurrence of a pyrite rich sulfide breccia at depth (Lehrmann et al. 2018, Murton et al. 2019).

Radiometric $^{230}Th/^{234}U$ dating of sulfides indicates that the MIR zone is the oldest sulfide zone within the TAG hydrothermal field, with activity starting ~100,000 years ago, which ceased around 600 years ago (Lalou et al. 1995). At the active TAG mound hydrothermal activity first started 50,000 years ago. Sulfides from the Shinkai mound yield ages of 23,000 - 2,000 years. Although thoroughly studied, no true resource estimates exist for the active TAG mound or the inactive mounds. However, based on the thickness of the sulfide zone derived from composite sections of the active mound Hannington et al. (1998) propose 2.7 million metric tons (Mt) of massive sulfides at 2% copper in the mound and additionally 1.5 Mt of sulfide breccia at 1% copper in the underlying stockwork zone.

Methodology

Sampling and petrological analyses

Surface and subsurface samples were collected during expedition JC138 on *RRS James Cook* using a robotic underwater vehicle (RUV HyBIS, National Oceanography Centre Southampton) and a robotic lander type seafloor drilling rig (RD2, British Geological Survey). In total, 29 surface samples and 9.5 m drill core were obtained from five hydrothermally inactive sites from the TAG hydrothermal field and after macroscopic description, 10 copper rich samples were selected for this study. Polished thick sections (200 μm) were prepared from the selected samples. These were visually characterised using optical and scanning electron microscopy (SEM) in backscattered electron mode and the mineral abundance was estimated optically.

EPMA and SEM element mapping

Quantitative analyses of major elements in the Cu rich sulfides, i.e. chalcopyrite, idaite, chalcocite, and covellite were carried out using a Cameca SX100 electron microprobe at the University of Edinburgh. In addition, a Zeiss Sigma HD Field Emission Gun Analytical SEM at Cardiff University was used to obtain high resolution X-ray element maps. Operating conditions for EPMA were an accelerating voltage of 20 kV and a beam current of 10nA and for SEM analyses an Oxford Instruments 150 mm^2 energy dispersive X-ray spectrometer was used with an accelerating potential of 15 kV. Calibration of EPMA and SEM was performed on natural mineral standards ($CuFeS_2$: Cu, S; FeS_2: Fe) monitoring the following spectral lines: Cu Kα, Fe Kα, S Kα. Wherever possible, spots were placed on areas free of visible inclusions or exsolutions of other minerals. Each spot location analysed was marked on a photomicrograph or backscatter electron image for later trace element analyses by LA-ICP-MS to ensure the analyses were made on the same grain.

LA-ICP-MS analyses

Trace elements were analysed by LA-ICP-MS using a New Wave UP 193 FX laser ablation system coupled to a Thermo Scientific X Series 2 quadrupole ICP-MS at the School of Ocean and Earth Science, University of Southampton. The laser used a mixed He (1 l/min) and N_2 (0.01 l/min) carrier gas, a beam diameter of 25 μm, a 5 Hz pulse rate with an energy density of 5-6 J/cm^2. The total analysis time for each spot was 45 s, including 20 s for gas blank analysis. In total 300 spots were analysed for chalcopyrite, 17 for idaite, 11 for chalcocite and 8 for covellite. 24 elements were monitored for quantitative analyses (^{51}V, ^{55}Mn, ^{57}Fe, ^{59}Co, ^{60}Ni, ^{65}Cu, ^{66}Zn, ^{69}Ga, ^{72}Ge, ^{75}As, ^{82}Se, ^{95}Mo, ^{107}Ag, ^{111}Cd, ^{115}In, ^{118}Sn, ^{121}Sb, ^{125}Te, ^{137}Ba, ^{197}Au, ^{205}Tl, ^{208}Pb, ^{209}Bi, ^{238}U) in addition to $^{77}ArCl$ and ^{83}Kr for interference correction on ^{82}Se. Calibration was achieved using NIST SRM 610 and NIST SRM 612 (Jochum et al. 2005) with Fe as an internal standard.

Accuracy was monitored by the repeated analysis of MASS-1 (Wilson et al. 2002) and is reported as percent relative differences (%RD). For the majority of elements, excellent accuracy was yielded, i.e. %RD of ± 0-3 (Jenner 1996). ^{60}Ni, ^{75}As, ^{115}In, ^{197}Au and ^{205}Tl show very good accuracy (between 3 and 7%) and only ^{82}Se and ^{111}Cd have poor accuracy of >10%. After measurement, the trace element concentrations were calculated with the PlasmaLab 2.6.1.335 software (Thermo Scientific) using Fe as internal standard as determined by EPMA. Mean minimum detection limits were calculated following the protocol of Longerich et al. (1996) and can be found in the Electronic Supplementary Materials (ESM), Table S1.

Results

Petrography

Three main seafloor massive sulfide sample types were identified in the surface and subsurface samples recovered (Table 1). They comprise chimney fragments (Fig. 2a), massive sulfides (Fig. 2b), and sulfide breccia (Fig. 2c). Chimney fragments are characterised by intact fluid conduits and the predominance of Cu rich sulfide minerals such as chalcopyrite and isocubanite. While the chalcopyrite displays various habits, ranging from tetrahedral to coarse grained anhedral (Fig. 2d-e), the isocubanite forms exsolution lamella (Fig. 2e). Other copper minerals that occur in the chimney fragments are idaite, which lines the inner fluid conduit, and covellite that formed along grain boundaries and micro-fractures (Fig. 2d, i). Massive sulfides and sulfide breccia predominately comprise pyrite which is either intercalated with chalcopyrite (Fig. 2f) or surrounds fossil remnants of tubular organism that got replaced by chalcopyrite (Fig. 2g). Along micro-fractures, chalcocite can be observed (Fig. 2h).

EPMA major element composition

The EPMA was performed to both confirm the identity of the secondary copper minerals and to provide iron concentrations to use as an internal standard for processing the LA-ICP-MS data. EPMA data show chalcopyrite from all sites to be stoichiometric $CuFeS_2$ with Cu and Fe concentrations varying from 32.78 to 35.40 wt.% and 29.72 to 31.81 wt.%, respectively (ESM, Table S2). A light orange to copper red coloured mineral that only occurs in chimney fragments from New Mound 2 was determined to be idaite (Fig. 3). In addition, the EPMA data show that the idaite (in this study) correlates well with the composition of idaite-II of Vaughan and Craig (1978) giving a stoichiometry of Cu_3FeS_4. Two blue coloured copper minerals with Cu concentrations of 77.70 to 78.27 wt.% and 65.31 to 67.62 wt.% are chalcocite (Cu_2S) and covellite (CuS). However, both minerals contain trace amounts of Fe (ESM, Table S2).

LA-ICP-MS trace element distribution

Though 24 elements were analysed by LA-ICP-MS in this study, only twelve of them will be discussed in detail (V, Mn, Co, Zn, Ga, Ge, As, Se, Mo, Ag, In, Sn, ESM Table S3 and S4). The other elements (Cd, Sb, Te, Au, Tl, Bi, U) yielded either values below the calculated, mean minimum detection limit or had concentrations of less than 1ppm. Significant Ba concentrations in some chalcopyrite grains reflect contamination by inclusions of barite and will not be considered any further. The elemental composition of chalcopyrite was studied considering different scales; within a single grain, across one sample, surface versus subsurface of one site, and between different sites.

Single grain scale

In comparison to other sulfides, such as pyrite and sphalerite, chalcopyrite crystals do not show optical zoning. A transect across a single chalcopyrite grain from a high temperature chimney fragment of New Mound 3 (Fig. 4) confirms this. Concentrations of Co, Zn, Ag and Mn across the grain are uniform yielding mean values of 160 ± 10 ppm, 70 ± 5 ppm, 31 ± 3 ppm and 44 ± 1 ppm, respectively. However, Se and Ge have heterogeneous compositions, with the highest values, 755 ppm Se and 2 ppm Ge, occurring in the centre of the grain; the overall range of those element concentrations stays within one order of magnitude. Concentrations of In show the opposite behaviour to those of Se and Ge, i.e., they decrease from the rim to the core. Though the concentrations of V are very low, ranging from 0.2 to 0.6 ppm, they show a depletion from one side of the chalcopyrite grain to the other. Mo and As concentrations are either very close to the detection limit or below.

Sample scale

Different generations of chalcopyrite occur within a chimney fragment from New Mound 2 (Fig. 5). Chalcopyrite 1 (Ccp1) is coarse grained and is associated with amorphous silica (blue). A second generation of chalcopyrite (Ccp2) forms a massive band and represents the outer layer of the fluid conduit wall. This chalcopyrite is associated with idaite. Separated by a thin band of marcasite the third generation of chalcopyrite (Ccp3) lines the inner walls of the conduit. Parts of this conduit are filled with goethite and very rare grains of sphalerite (not shown) occur.

Comparison of the trace element concentrations of three chalcopyrite generations of sample 55-1A (Ccp1, Ccp2, Ccp3) with chalcopyrite of the chimney fragment sample 55-6A are shown in Fig. 6. This chimney sample shows the highest concentrations of Se and Co (Fig. 6a-b). Average concentrations of 685 ± 158 ppm for Se and 178 ± 32 ppm for Co which are several orders of magnitude higher than the concentrations of Ccp1, Ccp2 and Ccp3 of the other chimney fragment 55-1A (ESM, Table S3). In addition, concentrations of Ag, In and Sn of chimney 55-6A are consistently higher than those measured in Ccp3 of chimney fragment 55-1A, but show very similar concentration in Ccp1 and Ccp2 (Fig. 6c-e). Concentrations of As, Ge, and Ga are consistently higher in Ccp3 of chimney 55-1A than in Ccp1 and Ccp2 of the same

chimney (Fig. 6f, h-i). The highest concentrations of Zn can be found in sample 55-6A and Ccp3 of sample 55-1A (Fig. 6j). However, Zn concentrations of more than 500 ppm are considered to come from the accident ablation of micro or nano inclusions of sphalerite. Concentration of V in Ccp1 and Ccp2 of sample 55-1A and in 55-6A is ≤5 ppm, whereas Ccp3 of sample 55-1A yields concentrations between 9 and 52 ppm (Fig. 6l).

Intra SMS mound variations and differences between mounds

As shown in the previous section, some chalcopyrite generations have 10s to 100s ppm of Se, Co and Ag incorporated, whereas other chalcopyrite are enriched in As, Ga, Ge and Mo. Chalcopyrite occurring in surface and subsurface samples of Southern mound (21-3B and 50-14) and from the deeper sample collected at MIR zone (73-29) shows elevated concentrations of Se (Fig. 7a). Co is only enriched in chalcopyrite from both Southern mound samples, yielding average values of 22 ± 2 ppm and 3 ± 1 ppm, but it does not show elevated concentrations in Rona mound and MIR zone (Fig. 7b). However, the measured concentrations are still two to three orders of magnitude lower than in chalcopyrite of chimney fragment 55-6A. All chalcopyrites from Rona mound and the shallower subsurface sample of the MIR zone (73-18) show similar concentrations of As, Mo, Ga and Ge to those determined in chimney fragment 55-1A-Ccp3 (Fig. 7f-i). By contrast, the Se rich chalcopyrite from Southern mound and the chimney fragment 55-6A exhibit the lowest concentrations of these elements with As being absent in 55-6A. The chimney fragments yield the highest concentrations of Ag (Fig. 7c). The shallower samples from Southern mound and Mir zone have higher concentrations of Ag than their deeper counterparts. All chalcopyrite from Rona mound show similar concentrations suggesting that concentrations are very similar to uniform within one hydrothermal site, though they differ between different sulfide mounds. This can also be observed for the elements In and Sn (Fig. 7d-e).

Finally, Zn concentrations in chalcopyrite from Southern mound and MIR zone appear to be uniform within the sulfide mounds and are one to two orders of magnitude lower than those determined in the chimney fragments 55-6A and 55-1A-Ccp3 (Fig. 7j). By contrast, samples from the Rona mound display a wider range, with the deeper samples 65-13 and 65-23 showing higher Zn concentrations possibly due to the presence of micro and nano inclusions of sphalerite.

Secondary copper minerals

Copper minerals other than chalcopyrite occur only in the surface samples (Table 1). In this study, three different secondary copper minerals were analysed. These are idaite from New Mound 2 (55-1A), chalcocite from Rona mound (45-7C) and covellite from Southern mound (21-3B) and New Mound 3 (55-6A). Due to the size of the minerals, only 36 spot analyses were performed. Covellite is characterised by high concentrations (100s to 1000s ppm) of Se and Co (Fig. 8a-b), low concentrations (<10 ppm) of Mo, Ge and Ga and the absence of As (Fig. 8f-i). Chalcocite and idaite have trace

elements incorporated that are found in chalcopyrite of Rona mound and chimney fragment 55-1A. While Co concentrations are low (<1 ppm) and Se low (<10 ppm) to absent, As, Ge, Mo, and Ga are present in concentrations of several 10s to 100s ppm (ESM, Table S4). Concentrations of Sn, Zn and Mn are relatively uniform in each mineral phase and do not differ between the different copper minerals (Fig. 8e,j,l). For In, with the exception of covellite from Southern mound, which shows average concentrations of 3 ± 1 ppm (Fig. 8d), the other copper minerals have average concentrations between 8 and 11 ppm. The highest concentrations of Ag are found in covellite from New Mound 3 (55-6A) and idaite from New Mound 2 (55-1A). Their average concentrations of 243 ± 23 ppm and 262 ± 62 ppm are one order of magnitude higher than in covellite from Southern mound (Fig. 8c) and two orders of magnitude higher than in chalcocite from Rona mound. Concentrations of V are lowest in covellite from Southern mound and New Mound 3 (Fig. 8k). Idaite exhibits slightly higher concentrations of V, whereas the highest concentrations are found in chalcocite from Rona mound, with an average concentration of 15 ± 7 ppm.

Discussion

Copper mineral assemblages and relative precipitation temperatures

Five Cu-(Fe)-sulfides were identified, which are hosted in three main sample types: (1) chimney fragments, (2) massive sulfides and (3) sulfide breccia. While chalcopyrite can be found in all three sample types, the occurrence of isocubanite and idaite is restricted to chimney fragments of New Mound 2 and 3. While chalcocite occurs only along micro-fractures, cutting through earlier chalcopyrite hosted in a sulfide breccia at Rona mound, covellite either lines the rims of chalcopyrite or idaite of chimney fragment samples or can be found filling micro-fractures in a massive sulfide sample of Southern mound.

Based on petrographic and textural observation and a comparison with published data from active and inactive SMS and ancient VMS systems, it is possible to assign relative formation and alteration temperatures to the different Cu-(Fe)-sulfides found in this study. Precipitation of chalcopyrite in SMS systems occurs at temperatures between >350 °C to 280 °C (Large 1992) with black smoker hydrothermal fluids at the active TAG hydrothermal vent yielding 370 °C (Tivey et al. 1995). Isocubanite, according to Large (1992), is also a high temperature Cu-(Fe)-sulfide, and formed through exsolution from chalcopyrite, with a temperature stability field ranging from 252 °C to 400 °C (Nenasheva and Kravchenko 2015). Idaite is quite rare in SMS systems, though its occurrence has been reported at the TAG mound and in VMS deposits of Cyprus (Constantinou 1975, Mozgova et al. 2000). The formation of the mineral is still not fully constrained. It has been proposed that idaite is a supergene alteration product of bornite (Frenzel 1959, Vaughan and Craig 1978), however, Constantinou (1975) proposed that the mineral formed through oxidative leaching of chalcopyrite by an acidic ferric rich solution that formed during the alteration of pyrite to goethite at low temperatures. Idaite from

New Mound 2 and 3 is associated with chalcopyrite, Fe poor sphalerite (Lehrmann et al. 2018) and goethite, i.e. a similar mineral assemblage to that of VMS deposits from Cyprus, and hence a low temperature formation is assumed for Ccp3 of chimney fragment 55-1A. The temperature window in which idaite is stable ranges from <256 °C to 50 °C (Wang 1984). Because of their distinctive association with isocubanite and idaite, chalcopyrite from chimney fragment 55-6a is of high temperature origin, whereas Ccp3 of 55-1A formed at low hydrothermal temperatures.

Chalcocite shows a monocline crystal system at temperatures of <103 °C but inverts into the hexagonal system at 103°C and remains in this crystal system to temperatures of ~435 °C (Fleet 2006). It is not known which crystal system the chalcocite of this study exhibits; however, based on its occurrence, it is clearly an alteration phase thus low formation temperatures are considered most likely. Covellite can be stable at temperatures of up to 507 °C (Fleet 2006). In this study, however, covellite is clearly a secondary alteration phase as it is lining the rims and fractures of earlier idaite and chalcopyrite. Hence, its formation temperature is likely to be in the range of those from idaite.

Trace element budget of chalcopyrite

Despite chalcopyrite being the predominant source for copper, one would assume that the valence state of Cu and Fe, which occupies the cation sites of the mineral structure, is known; however, there is ongoing debate as to the valence state of these elements. While Todd et al. (2003) propose Cu and Fe to be divalent ($Cu^{2+}Fe^{2+}S_2^{2-}$), Pearce et al. (2006) suggest Cu to be monovalent and Fe to be trivalent ($Cu^{+}Fe^{3+}S_2^{2-}$). However, Li et al. (2013) suggested that due to covalent bonding of atoms in the structure of chalcopyrite, an intermediate valence state is valid, i.e. both valence states for Cu and Fe are present. Because of this uncertainty, mechanisms for trace element incorporation are more complex and highly dependent on the presence or absence of co-crystallising sulfides (George et al. 2016) and fluid temperature (Seyfried and Ding 1995, Schmidt et al. 2007). In general, trace elements can be hosted in a mineral in three different ways: (1) structurally bound in the mineral lattice, (2) as micro and nano inclusions, or (3) adsorbed to the surface of the mineral. Wohlgemuth-Ueberwasser et al. (2015) noted that LA-ICP-MS is unable to distinguish between lattice bound elements and uniformly distributed nano inclusions within a mineral due to the size of the spot. This is also valid within this study where we used an ablation spot size of 25 μm.

Chalcopyrite associated with isocubanite is thought to be of high temperature origin and is characterised by high concentrations of Se and Co (Fig. 9a). While Se substitutes for S (Huston et al. 1995), Co gets incorporated into the position of Fe (George et al. 2018). The temperature window for Se and Co incorporation into the structure of chalcopyrite is >300 °C, or even ~350 °C (Auclaire et al. 1987, Huston et al. 1995). According to Metz and Trefry (2000), there is a sharp drop in Co concentrations in the vent fluid at <350 °C, with Liu et al. (2011) suggesting that Co and Cu concentrations are very low at temperatures of <250 °C. This would explain why the mineral assemblage in black smoker

precipitates is dominated by chalcopyrite.; However, in precipitates from white smokers, sphalerite is predominant,with chalcopyrite being only an accessory phase. As high fluid temperatures are needed to transport Se, it is considered to be immobile during recrystallisation events as long the temperatures do not exceed 300 °C. Overall, this suggests that not only chalcopyrite of New Mound 3 (55-6A) formed at high temperatures, but also chalcopyrite from both Southern mound samples and the deeper sub-seafloor sample from MIR zone (73-29).

The highest concentrations of Ag occur in the chimney fragment 55-6A (Fig. 9a) and are several orders of magnitude higher than in any other analysed chalcopyrite. In general, Ag substitutes for Cu (Huston et al. 1995, George et al. 2018). In the previous section (Fig. 7c) the hypothesis was that Ag concentrations are linked to high formation temperature. This would explain the Ag rich chalcopyrite of chimney fragment 55-6A, but it does not explain why concentrations of Ag in the other chalcopyrite samples from Southern mound and MIR zone record low concentrations. This suggests a different explanation. One hypothesis is that Ag concentrations are linked to the occurrence of isocubanite which was only identified in sample 55-6A. Another hypothesis is that the occurrence of Ag is linked to the sample type, i.e., even the chalcopyrite hosted in the chimney fragment of 55-1A has higher Ag than any other Cu-(Fe)- sulfide found in the massive sulfide and sulfide breccia samples. Other chimney samples analysed by Butler and Nesbitt (1999), Maslennikov et al. (2009), Wohlgemuth-Ueberwasser et al. (2015), and Melekestseva et al. (2017) confirm the presence of Ag in chalcopyrite. Alternatively, an explanation could be the paragenetic stage of the samples; the chimney fragments being the youngest, i.e., less altered, whereas the samples from the other sulfide mounds have undergone low and high temperature alteration which changed the trace metal budget.

The trace elements In, Sn, As, Ga, Ge, Mo, and Zn are thought to be able to incorporate into the lattice of chalcopyrite by either direct or coupled substitution, predominately partitioning into the Fe site and to a minor degree the Cu site (Huston et al. 1995, Maslennikov et al. 2009, George et al. 2016, 2018, Grant et al. 2018). While the window of incorporation into the lattice of chalcopyrite for Sn, In and Mo is considered to be in the medium to high temperature range (Maslennikov et al. 2009, Monecke et al. 2016), As, Ga, Ge and Zn occur in chalcopyrite that formed at low to medium temperatures (Metz and Trefry 2000, Maslennikov et al. 2009, Monecke et al. 2016). All samples from Southern mound, the deeper MIR zone and the chimney fragment that were considered to be of high temperature origin exhibit Mo concentrations that are either below the mean detection limit (Fig. 9c) or are one to two orders of magnitude lower than concentrations found in Ccp3 from the inner chimney orifice (55-1A), Rona mound samples and the shallower sample of MIR zone (73-18). A similar pattern can be observed for Ga, As and Ge which are also enriched in the Rona mound and chalcopyrite from New Mound 2 (Fig. 9b,d). The high Ga and Sn concentrations only found in chalcopyrite of Rona mound are not only related to the lower fluid temperature but also to the occurrence of sphalerite in the shallower part of the subsurface (Lehrmann

et al. 2018). George et al. 2018 suggest that Ga and Sn can be remobilised from pre-existing sphalerite and incorporated into the chalcopyrite.

Zn is not only hosted in the lattice of chalcopyrite but it can also occur as inclusions. Kojima and Sugaki (1985) propose that up to 1800 ppm can be incorporated into the chalcopyrite at 300 °C, however maximum Zn concentrations related to incorporation into the chalcopyrite lattice are 235 ppm (Fig. 9e). Everything above this value is thought to be related to Zn bearing mineral inclusions.

Vanadium is neither known to be incorporated into the lattice of the chalcopyrite nor to form inclusions, but rather gets absorbed onto the mineral surface (Butler and Nesbitt 1999) with V originating from cold seawater. Once the V is fixed to the surface, it is very difficult to remobilise (Butler and Nesbitt 1999). Concentrations of V are quite constant within different chalcopyrite samples. Two exceptions are from the surface of Rona mound and Ccp3 of 55-1A (Fig. 9f). The reason why those two samples yield V concentrations of more than one order of magnitude higher to those in the other samples can be explained by the rock type they are hosted in. Chalcopyrite of 45-7C occurs within a sulfide breccia where it is heavily pervaded by micro-fractures that act as pathways for seawater ingress. The other V rich chalcopyrite is found in the inner conduit of a chimney, which is naturally more permeable than massive sulfide blocks. Goethite that precipitated within the inner conduit confirms that the chimney sample 55-1A underwent seafloor weathering, and hence extensive exposure to seawater. In this way, V can be used as a useful tracer of seawater interaction within SMS deposits (Butler and Nesbitt 1999 and references therein). Manganese is highly soluble in reduced fluids at high temperature, thus does not precipitate (Maslennikov et al. 2009). However, at low temperatures and in oxygenated conditions, it precipitates directly from a hydrothermal fluid or adsorbed from seawater onto a mineral surface (Grant et a. 2018). Chalcopyrite hosted in samples taken from the surface of sulfide mounds exhibit concentrations that are one order of magnitude higher than those from the subsurface (Fig. 9f), suggesting the absorption of seawater derived Mn. Several analyses of chalcopyrite hosted in subsurface samples exhibit very high Mn concentrations of several 100s ppm. However, these chalcopyrite are Se and/or Co rich chalcopyrite, i.e., formed at high temperatures, hence cannot be related to surface adsorption. Thus, they are assumed to be related to Mn rich mineral inclusions. While some high Mn concentrations correlate with high Zn, for others, no correlation exists with any of the discussed elements.

Secondary copper alteration minerals

The predominant oxidation stage in the copper minerals idaite (Cu_3FeS_4), chalcocite (Cu_2S) and covellite (CuS) is monovalent for Cu and trivalent for Fe (Fleet 2006). The identical valence states of Cu and Fe in the secondary copper minerals to those in chalcopyrite mean that similar element distributions are expected in the alteration phases. Those elements that are only mobile at high temperatures, e.g. Se will also be retained in low temperature alteration phases. In comparison to chalcopyrite of the inner (Ccp3) and outer (Ccp2) conduit of sample 55-1A, idaite exhibits trace element

concentrations that fall between those of the other two chalcopyrite generations (Fig. 10a). The exceptions are Mo and Ag that are enriched in idaite by one to two orders of magnitude to those in Ccp2 and Ccp3. In addition, Co and Mn concentrations are almost identical in the chalcopyrite and idaite and V shows higher concentration in Ccp3 than Ccp2 and the idaite.

Chalcocite does not differ significantly with regard to its trace element pattern in comparison to earlier paragenetic chalcopyrite (Fig. 10b). As with idaite only Ag and Mo are enriched. Covellite from Southern mound and New Mound 3 are also enriched in Mo and Ag in comparison to associated chalcopyrite (Fig. 10c-d). Other elements enriched in covellite from Southern mound are V and Se. While higher concentrations of V can be explained by exposure to seawater that entered the mineral structure through micro-fractures, the high Se concentration exhibited in the covellite is inherited from the precursor chalcopyrite as a low temperature fluid cannot mobilise nor precipitate Se (Genna and Gaboury 2015). Overall, Ag and Mo appear to be the elements getting incorporated into the lattice of secondary copper minerals during alteration, with Ag substituting for monovalent Cu. The elevated concentration of Ag in chalcocite suggests that the mineral has a monovalent crystal structure and thus formed at temperatures of <103 °C as hexagonal chalcocite, which formed at higher temperature is Ag poor (Cook et al. 2011). Although the end members covellite and chalcocite do not host any Fe according to Vaughan and Craig (1978), here, up to percent level concentrations of Fe play an important role allowing the substitution of trivalent Fe by trivalent Mo which has almost the same ionic radius.

Source of trace elements

In general, it is proposed that chemical composition and mineralogy of SMS deposits vary in different tectonic settings, which have a specific geology and composition of hydrothermal fluids (Hannington et al. 2005). Key parameters influencing the composition of the hydrothermal fluid are source rock composition and input of magmatic volatiles (Hannington et al. 2005). Mafic to ultramafic systems are known to be Cu and Co rich, whereas felsic systems are enriched in Zn, As, Sb, and Pb (Hannington et al. 2005, Monecke et al. 2016). The TAG mound is a basalt hosted system and basalt is expected to underlie the other sulfide mounds investigated here, hence a similar trace element pattern should be observed in the various chalcopyrite grains. To decipher the origin of the trace elements in chalcopyrite requires trace element data for source rock, seawater and hydrothermal vent fluids. However, available vent fluid data from the TAG mound or elsewhere do not include data for concentrations of V, Ga, Ge, Se, As, and Sn (Douville et al. 2002). Primitive mantle normalised mean trace element patterns of the high and low temperature chimney fragments from 55-6A (New Mound 3) and 55-1A-Ccp3 (New Mound 2) are quite distinctive (Fig. 11a). While Se, Ag, In, and Sn are enriched in the high temperature chimney fragment with respect to primitive mantle, elements that originate from seawater such as V and Mn are depleted. In the low temperature chimney fragment, V concentrations are two orders of magnitude higher than in

chalcopyrite from the high temperature chimney, suggesting that this chimney fragment has had longer exposure to seawater. Other elements that are enriched are the intermediate to low temperature elements As, Ge, Ga, and Mo. Seawater Mo concentrations are 10.1 parts per billion (Douville et al. 2002) and therefore 21 times higher than in the hydrothermal fluid at TAG. The presence of Mo suggests that ascending hydrothermal fluid mixed with seawater. Normalised mean trace element patterns of chalcopyrite from Southern mound surface and subsurface are very similar (Fig. 11b) with the exception of slightly higher concentrations of V and Mn which suggest a longer exposure to seawater. In addition, both samples have different concentrations of Mo and Ag, with the surface sample exhibiting lower concentrations of Mo and higher concentrations of Ag than those of the subsurface. The lower concentrations of Mo could either indicate that the element was not precipitated and lost by emission through the vent, was precipitated in an associated mineral phase, was depleted in the vent fluid or was removed from the mineral structure during a later hydrothermal stage. The trace element patterns of chalcopyrite from Rona mound are consistent (Fig. 11c). The surface sample exhibits the highest concentrations of V and Mn and correlates well with extended exposure to seawater (as well as having the lowest concentration of Sn). Sn is presumed to originate from recrystallisation of earlier precipitated sphalerite, hence the higher Sn concentrations observed in all subsurface chalcopyrite. Interestingly, the shallowest subsurface sample from Rona mound (65-9) shows the lowest concentration of V and Mo, whereas concentrations found in deeper parts of the mound are higher. This suggests that below the sample location of 65-9, the mound is cut by a fracture that allows ingress of seawater to the deeper part without affecting the composition of the shallower chalcopyrite. The existence of such fractures was confirmed visually during expedition JC138 (Murton et al. 2019). Chalcopyrite from the shallower subsurface sample of MIR zone shows higher concentrations of seawater derived V and Mo and lower concentrations of Se and Sn (Fig. 11d). The absence of a sphalerite rich zone at the MIR zone suggests the Sn is unlikely to have originated from earlier precipitated sphalerite and is assumed to have precipitated directly from the vent fluid.

Conclusions

- In the absence of co-precipitating sulfides, hydrothermal chalcopyrite can incorporate a diverse trace element suite up to several hundreds of ppm that represent different formation, remobilisation and alteration stages.
- Trace element concentrations of chalcopyrite do not only vary between different chalcopyrite generations within one sample, but also show variations from surface to subsurface within a single sulfide mound. In addition, chalcopyrite from different mounds show distinguishable concentrations of certain trace elements.
- The incorporation of trace elements is dependent on a change in the physicochemical conditions. Contrary to previous expectations, the host rock composition plays only a minor role with regard to the trace element budget.

- Typical high temperature indicators are high concentrations of Se, Co and to a certain degree Ag. As, Ga, and Ge are found in chalcopyrite that formed at low temperatures with Ga and Sn originating from earlier precipitated sphalerite at some sites. Exposure to seawater can be identified by elevated concentrations of Mo, Mn and V.
- Secondary copper minerals display very similar trace element patterns to the primary chalcopyrite, with high temperature element signatures often being retained. Elevated concentrations of Ag and Mo suggest that these elements substitute, due to similar ionic radii into the site of the monovalent Cu and trivalent Fe. Due to micro-fractures and hence increased permeability, V and Mn concentrations can be higher in the secondary phase because of alteration.
- The absence of certain trace elements suggests that an element either was depleted in the vent fluid, escaped through a vapour phase or got leached from the mineral and reprecipitated elsewhere in the sulfide mound.

Acknowledgements

We wish to thank the officers and crew of *RRS James Cook* and the shipboard technical party for their professionalism and constant support during expedition JC138. Thanks also to D. Doran and M. Beverley-Smith (University of Southampton), D. Muir (Cardiff University) and C. Hayward (University of Edinburgh) for section preparation and technical support of the SEM and EPMA. Helpful comments by two anonymous reviewers and A.E. Cabral are gratefully acknowledged. We also wish to extend our thanks and appreciation to editor-in-chief Georges Beaudoin.

Funding

This study was funded by a grant from the European Union Seventh Framework Program (EU-FP7) "Blue Mining: breakthrough solutions for the sustainable deep-sea mining value chain" under grant No. 604500. The grant also supported the cruise on the NERC ship *RRS James Cook* (JC138) in 2016.

Declarations

Conflicts of interest/Competing interests

The authors have no conflicts of interest to declare that are relevant to the content of this article.

Availability of data and material

The complete analytical data set is included in the electronic supplementary material.

Code availability

Not applicable

References

Auclair G, Fouquet Y, Bohn M (1987) Distribution of selenium in high-temperature hydrothermal sulfide deposits at 13°N, East Pacific Rise. Can Mineral 25:577–587.

Beaulieu SE, Baker ET, German CR (2015) Where are the undiscovered hydrothermal vents on oceanic spreading ridges? Deep-Sea Res II Top Stud Oceanogr 121:202–212. https://doi.org/10.1016/j.dsr2.2015.05.001

Butler IB, Nesbitt RW (1999) Trace element distributions in the chalcopyrite wall of a black smoker chimney; insights from laser ablation inductively-coupled plasma mass spectrometry (LA-ICP-MS). Earth Planet Sci Lett 167:335–345. https://doi.org/10.1016/S0012-821X(99)00038-2

Constantinou C (1975) Idaite from the Skouriotissa Massive Sulfide Orebody, Cyprus: Its Composition and Conditions of Formation. Am Mineral 60:1013-l018.

Cook NJ, Ciobanu CL, Danyushevsky LV, Gilbert S (2011) Minor and trace elements in bornite and associated Cu–(Fe)-sulfides: A LA-ICP-MS study. Geochim Cosmochim Acta 75:6473–6496. https://doi.org/10.1016/j.gca.2011.08.021

Dekov VW, Garbe-Schönberg D, Kamenov GD, Gueguen B, Bayon G, Bindi L, Asael D, Fouquet Y (2018) Redox changes in a seafloor hydrothermal system recorded in hematite-chalcopyrite chimneys. Chem Geol 483:351–371. https://doi.org/10.1016/j.chemgeo.2018.02.041

Douville E, Charlou J-L, Oelkers EH, Bienvenu P, Jove Colon CF, Donval JP, Fouquet Y, Prieur D, Appriou P (2002) The rainbow vent fluids (36°14′N, MAR): the influence of ultramafic rocks and phase separation on trace metal content in Mid-Atlantic Ridge hydrothermal fluids. Chem Geol 184:37–48. https://doi.org/10.1016/S0009-2541(01)00351-5

Fleet ME (2006) Phase equilibria at high temperatures. Rev Mineral Geochem 61:365–419. https://doi.org/10.2138/rmg.2006.61.7

Frenzel G (1959) Idaite und blaubleibender Covellin. Neues Jahrb mineral Abh 93:87-132.

Genna D, Gaboury D (2015) Deciphering the hydrothermal evolution of a VMS system by LA-ICP-MS using trace elements in pyrite: an example from the Bracemac-McLeod deposits, Abitibi, Canada, and implications for exploration. Econ Geol 110:2087–2108. http://dx.doi.org/10.2113/econgeo.110.8.2087

George LL, Cook NJ, Ciobanu CL (2016) Partitioning of trace elements in co-crystallized sphalerite-galena-chalcopyrite hydrothermal ores. Ore Geol Rev 77:97–116. https://doi.org/10.1016/j.oregeorev.2016.02.009

George LL, Cook NJ, Crowe BBP, Ciobanu CL (2018) Trace elements in hydrothermal chalcopyrite. Mineral Mag 82:59–88. https://doi.org/10.1180/minmag.2017.081.021

461 Grant HLJ, Hannington MD, Petersen S, Frische M, Fuchs SH (2018) Constraints on the behavior of trace elements in
462 the actively-forming TAG deposit, Mid-Atlantic Ridge, based on LA-ICP-MS analyses of pyrite. Chem Geol 498:45-
463 71. https://doi.org/10.1016/j.chemgeo.2018.08.019
464 Hannington MD, Herzig PM, Scott S, Thompson G, Rona P (1991) Comparative mineralogy and geochemistry of gold-
465 bearing sulfide deposits on the mid-ocean ridges. Mar Geol 101:217–248. https://doi.org/10.1016/0025-3227(91)90073-
466 D
467 Hannington MD, Galley AG, Herzig PM, Petersen S (1998) Comparison of the TAG mound and stockwork complex
468 with Cyprus-type massive sulfide deposits. In: Herzig PM, Humphris SE, Zierenberg RA (eds) Proc ODP Sci Results,
469 College Station, TX (Ocean Drilling Program) 158:389–415.
470 Hannington MD, de Ronde CEJ, Petersen S (2005) Sea-floor tectonics and submarine hydrothermal systems. In:
471 Hedenquist JW et al. (eds) Econ Geol 100th Anniv Vol 111–141. https://doi.org/10.5382/AV100.06
472 Hannington MD, Jamieson J, Monecke T, Petersen S, Beaulieu S (2011) The abundance of seafloor massive sulfide
473 deposits. Geol 39:1155–1158. https://doi.org/10.1130/G32468.1
474 Humphris SE, Tivey MK, Tivey MA (2015) The Trans-Atlantic Geotraverse hydrothermal field: a hydrothermal system
475 on an active detachment fault. Deep-Sea Res II Top Stud Oceanogr 121:8–16.
476 https://doi.org/10.1016/j.dsr2.2015.02.015
477 Huston DL, Sie S-H, Suter GF, Cooke DR (1995) Trace elements in sulfide minerals from Eastern Australian volcanic-
478 hosted massive sulfide deposits: part I. proton microprobe analyses of pyrite, chalcopyrite, and sphalerite, and part II.
479 selenium levels in pyrite: comparison with δ34S values and implications for the source of sulfur in volcanogenic
480 hydrothermal systems. Econ Geol 90:1167–1196. http://dx.doi.org/10.2113/gsecongeo.90.5.1167
481 Jenner GA (1996) Trace element geochemistry of igneous rocks: geochemical nomenclature and analytical
482 geochemistry. In: Wyman D (ed) Trace element geochemistry of volcanic rocks: applications for massive sulfide
483 exploration. Geol Assoc Can 12:51-77.
484 Jochum KP, Nohl U, Herwig K, Lammel E, Stoll B, Hofmann AW (2005) GeoReM: A New Geochemical Database for
485 Reference Materials and Isotopic Standards. Geostand Geoanal Res 29:333-338. 10.1111/j.1751-908X.2005.tb00904.x
486 Keith M, Häckel F, Haase KM, Schwarz-Schampera U, Klemd R (2016) Trace element systematics of pyrite from
487 submarine hydrothermal vents. Ore Geol Rev 72:728–745. https://doi.org/10.1016/j.oregeorev.2015.07.012
488 Kojima S and Sugaki A (1985) Phase relations in the Cu–Fe–Zn–S system between 500° and 300 °C under
489 hydrothermal conditions. Econ Geol 80:158–171. https://doi.org/10.2113/gsecongeo.80.1.158

Lalou C, Reyss JL, Brichet E, Rona PA, Thompson G (1995) Hydrothermal activity on a 10^5-year scale at a slow-spreading ridge, TAG hydrothermal field, Mid-Atlantic Ridge 26°N. J Geophys Res 100:17855–17862. https://doi.org/10.1029/95JB01858

Large RR (1992) Australian volcanic-hosted massive sulfide deposits: Features, styles and genetic models. Econ Geol 87:471–510. https://doi.org/10.2113/gsecongeo.87.3.471

Lehrmann B, Stobbs IJ, Lusty PAJ, Murton BJ (2018) Insights into Extinct Seafloor Massive Sulfide Mounds at the TAG, Mid-Atlantic Ridge. Mineral 8: 302. https://doi.org/10.3390/min8070302

Li Y, Kawashima N, Li J, Chandra AP, Gerson AR (2013) A review of the structure, and fundamental mechanisms and kinetics of the leaching of chalcopyrite. Adv Colloid Interface Sci 197:1–32. https://doi.org/10.1016/j.cis.2013.03.004

Liu W, Borg SJ, Testemale D, Etschmann B, Hazemann J-L, Brugger J (2011) Speciation and thermodynamic properties for cobalt chloride complexes in hydrothermal fluids at 35–440 °C and 600 bar: an in-situ XAS study. Geochim Cosmochim Acta 75:1227–1248. https://doi.org/10.1016/j.gca.2010.12.002

Longerich HP, Jackson SE, Günther D (1996) Laser Ablation Inductively Couples Plasma Mass Spectrometric Transient Signal Data Acquisition and Analyte Concentration Calculation. J Anal At Spectrom 11:899-904. https://doi.org/10.1039/JA9961100899

Maslennikov VV, Maslennikova SP, Large RR, Danyushevsky L (2009) Study of Trace Element zonation in vent chimneys from the Silurian Yaman-Kasy volcanic hosted massive sulfide deposit (Southern Urals, Russia) using laser ablation-inductively coupled plasma mass spectrometry (LA-ICPMS). Econ Geol 104:111–141. https://doi.org/10.2113/gsecongeo.104.8.1111

Maslennikov VV, Cherkashov G, Artemyev DA, Firstova A, Large RR, Tseluyko A, Kotlyarov V (2020) Pyrite Varieties at Pobeda Hydrothermal Fields, Mid-Atlantic Ridge 17°07'–17°08' N: LA-ICP-MS Data Deciphering. Mineral 10:622. https://doi.org/10.3390/min10070622

Melekestseva IY, Maslennikov YV, Tret'yakov GA, Maslennikova SP, Danyushevsky LV, Kotlyyarov V, Large RR Beltenev VE, Khvorov P (2020) Trace Element Geochemistry of Sulfides from the Ashadze-2 Hydrothermal Field (12°58'N, Mid-Atlantic Ridge): Influence of Host Rocks, Formation Conditions or Seawater? Mineral 10: 743. https://doi:10.3390/min10090743

Melekestseva IY, Maslennikov YV, Tret'yakov GA, Nimis P, Beltenev VE, Rozhdestvenskaya II, Maslennikova SP, Belogub EV, Danyushevsky LV, Large RR, Yuminov AM, Sadykjov SA (2017) Gold- and silver-rich massive sulfides from the Semenov-2 hydrothermal field, 13°31.13′ N, Mid-Atlantic Ridge: a case of magmatic contribution? Econ Geol 112: 741–773. http://dx.doi.org/10.2113/econgeo.112.4.741

520 Melekestseva IY, Tret'yakov GA, Nimis P, Yuminov AM, Maslennikov YV, Maslennikova, SP, Kotlyarov VA,
521 Beltenev VE, Danyushevsky LV, Large RR (2014) Barite-rich massive sulfides from the Semenov-1 hydrothermal field
522 (Mid-Atlantic Ridge, 13°30.87′ N): Evidence for phase separation and magmatic input. Mar Geol 349:37–54.
523 https://doi.org/10.1016/j.margeo.2013.12.013
524 Meng X, Li X, Chu F, Zhu J, Lei J, Li Z, Wang H, Chen L, Zhu Z (2020) Trace element and sulfur isotope
525 compositions for pyrite across the mineralization zones of a sulfide chimney from the East Pacific Rise (1–2° S). Ore
526 Geol Rev 116:1–15. https://doi.org/10.1016/j.oregeorev.2019.103209
527 Metz S, Trefry JH (2000) Chemical and mineralogical influences on concentrations of trace metals in hydrothermal
528 fluids. Geochim Cosmochim Acta 64:2267–2279. https://doi.org/10.1016/S0016-7037(00)00354-9
529 Monecke T, Petersen S, Hannington MD, Grant HLJ, Samson IM (2016) The Minor Element endowment of modern
530 sea-floor massive sulfides and comparison with deposits hosted in ancient volcanic successions. Rev Econ Geol
531 18:245–306. https://doi.org/10.5382/Rev.18.11
532 Mozgova NN, Borodaev YS, Stepanova TV, Cherkashev GA, Zhirnov EA (2000) Noble Metals in Sulfide Assemblages
533 from Deep Sectors of the Active TAG Mound (Mid-Atlantic Ridge, 26°08' N). Lithol Mineral Res 35:1-18.
534 https://doi.org/10.1007/BF02788281
535 Mudd GA, Jowitt SM, Werner TT (2017) The world's by-product and critical metal resources part I: Uncertainties,
536 current reporting practices, implications and grounds for optimism. Ore Geol Rev 86:924-938.
537 http://dx.doi.org/10.1016/j.oregeorev.2016.05.001
538 Murton BJ, Lehrmann B, Dutrieux AM, Martins S, Gil de la Iglesia A, Stobbs IJ, Barriga FJAS, Bialas J, Dannowski A,
539 Vardy ME, North LJ, Yeo IALM, Lusty PAJ, Petersen S (2019) Geological fate of seafloor massive sulphides at the
540 TAG hydrothermal field (Mid-Atlantic Ridge). Ore Geol Rev 107:903–925.
541 https://doi.org/10.1016/j.oregeorev.2019.03.005
542 Nenashevaa SN, Kravchenkob TA (2015) Composition Features of Isocubanite and Polymorphous Modifications of
543 $CuFe_2S_3$. Compd Geol Ore Depos 57:626–633. https://doi.org/10.1134/S1075701515070090
544 Palme H, O'Neill HStC (2014) Cosmochemical Estimates of Mantle Composition. Treatise on Geochemistry 2nd
545 Edition 3:1-39. http://dx.doi.org/10.1016/B978-0-08-095975-7.00201-1
546 Pearce CI, Pattrick RAD, Vaughan DJ, Henderson CMB, Van der Laan G (2006) Copper oxidation state in
547 chalcopyrite: Mixed Cu d^9 and d^{10} characteristics. Geochim Cosmochim Acta 70:4635–4642.
548 https://doi.org/10.1016/j.gca.2006.05.017
549 Rankin, WJ (2017) Sustainability – the role of mineral processing and extractive metallurgy. Mineral Process Extr
550 Metall 126:3-10. https://doi.org/10.1080/03719553.2016.1264164

Rona PA, Klinkhammer G, Nelsen TA, Trefry JH, Elderfield H (1986) Black smokers, massive sulfides, and vent biota at the Mid-Atlantic Ridge. Nat 321:33–37. https://doi.org/10.1038/321033a0

Rona PA, Bogdanov YA, Gurvich EG, Rimski-Korsakov A, Sagalevitch AM, Hannington MD, Thompson G (1993) Relict hydrothermal zones in the TAG hydrothermal field, Mid-Atlantic Ridge 26°N, 45°W. J Geophys Res 98:9715–9730. https://doi.org/10.1029/93JB00552

Schmidt K, Koschinsky A, Garbe-Schönberg D, de Carvalho LM, Seifert R (2007) Geochemistry of hydrothermal fluids from the ultramafic-hosted Logatchev hydrothermal field, 15°N on the Mid-Atlantic Ridge: temporal and spatial investigation. Chem Geol 242:1–21. https://doi.org/10.1016/j.chemgeo.2007.01.023

Seyfried WE, Ding K (1995) Phase Equilibria in Subseafloor Hydrothermal Systems: A Review of the Role of Redox, Temperature, pH and Dissolved Cl on the Chemistry of Hot Spring Fluids at Mid-Ocean Ridges. In: Humphris SR, Zierenberg RA, Mullineaux LS, Thomson RE (eds) Seafloor Hydrothermal Systems, Physical, Chemical, Biological, and Geological Interactions. Geophy Monog 91:248–272. https://doi.org/10.1029/GM091p0248

Singer DA (2014) Base and precious metal resources in seafloor massive sulfide deposits. Ore Geol Rev 56:66-72. http://dx.doi.org/10.1016/j.oregeorev.2013.11.008

Stepanova TV, Krasnov SG, Cherkashev GA (1996) Mineralogy, chemical composition and structure of the MIR mound, TAG hydrothermal field. Geophys Res Lett 23:3515-3518. https://doi.org/10.1029/96GL02145

Tivey MK, Humphris SE, Thompson G, Hannington MD, Rona PA (1995) Deducing patterns of fluid flow and mixing within the TAG active hydrothermal mound using mineralogical and geochemical data. J Geophys Res 100:12,527–12,555. https://doi.org/10.1029/95JB00610

Tivey MA, Schouten H, Kleinrock MC (2003) A near-bottom magnetic survey of the Mid-Atlantic Ridge axis at 26°N: implications for the tectonic evolution of the TAG segment. J Geophys Res 112:2277. https://doi.org/10.1029/2002JB001967

Todd EC, Sherman DM, Purton JA (2003) Surface oxidation of chalcopyrite ($CuFeS_2$) under ambient atmospheric and aqueous (pH 2–10) conditions: Cu, Fe L- and O K-edge X-ray spectroscopy. Geochim Cosmochim Acta 67:2137–2146. https://doi.org/10.1016/S0016-7037(02)01371-6

Vaughan DJ, Craig JR (1978) Mineral chemistry of metal sulfides. Cambridge University Press

Wang N (1984) A contribution to the Cu-Fe-S system: the sulfidation of bornite at low temperatures. Neues Jahrb Mineral 8:346-352.

Wang Y, Han XH, Petersen S, Frische M, Qiu Z, Li H, Wu Z, Cui R (2017) Mineralogy and trace element geochemistry of sulfide minerals from the Wocan Hydrothermal Field on the slow-spreading Carlsberg Ridge, Indian Ocean. Ore Geol Rev 84:1–19. https://doi.org/10.1016/j.oregeorev.2016.12.020

Wang M, Feng C (2019) Decoupling economic growth from carbon dioxide emissions in China's metal industrial sectors: A technological and efficiency perspective. Sci Total Environ 691:1173-1181. https://doi.org/10.1016/j.scitotenv.2019.07.190

White SN, Humphris SE, Kleinrock MC (1998) New observations on the distribution of past and present hydrothermal activity in the TAG area of the Mid-Atlantic Ridge (26°08'N). Mar Geophys Res 20:41–56. https://doi.org/10.1023/A:1004376229719

Wilson S, Ridley W, Koenig A (2002) Development of sulfide calibration standards for the laser ablation inductively-coupled plasma mass spectrometry technique. J Anal At Spectrom 17:406–409. https://doi.org/10.1039/B108787H

Wohlgemuth-Ueberwasser C, Viljoen F, Petersen S, Vorster C (2015) Distribution and solubility limits of hydrothermal black smoker sulfides: an in-situ LA-ICP-MS study. Geochim Cosmochim Acta 159:16–41. https://doi.org/10.1016/j.gca.2015.03.020

Yuan B, Hongjun Y, Yang Y, Zhao Y, Yang J, Xu Y, Lin Z, Tang X (2018) Zone refinement related to the mineralization process as evidenced by mineralogy and element geochemistry in a chimney fragment from the Southwest Indian Ridge at 49.6°E. Chem Geol 482:46–60. https://doi.org/10.1016/j.chemgeo.2018.01.024

Table captions

Table 1 Sample list for analysed Cu-(Fe)-sulfides and their estimated mineral abundance

Abbreviations: -- absent, o trace (≤1%), x minor (1-5%), + common (5-25%), ++ abundant (25-50%), +++ dominant (≥50%); Ccp (chalcopyrite), Cct (chalcocite), Cv (covellite), Id (idaite), Iso (isocubanite), Mrc (marcasite), Py (pyrite), Sp (sphalerite), Others include holes, silicates, barite, jarosite, atacamite and iron-oxyhydroxides

Figure captions

Fig. 1 Bathymetric map of the TAG hydrothermal field and its active and inactive hydrothermal sites (data source GeoMapApp: KN142-05 (TAG94), DSL120 2m grid White). The inset shows the location on the Mid-Atlantic

Fig. 2 Images and reflected light photomicrographs of representative surface and sub-surface sulfide samples from inactive seafloor massive sulfides sites from the TAG hydrothermal field; a: chimney fragment predominately composed of chalcopyrite and marcasite with a visible fluid conduit (55-1A), b: massive sulfide composed of pyrite with intercalated chalcopyrite and partial brecciation at the sample rim (21-3B), c: sulfide breccia composed of pyrite crossed by a band of chalcopyrite (73-29), d: cross section of a chimney fluid conduit composed of two generations of chalcopyrite and subhedral idaite showing alteration to covellite; rare sphalerite and goethite occur in the orifice (55-1A), e: chalcopyrite

with exsolution lamella of isocubanite (55-6A), f: two generations of pyrite with intercalated chalcopyrite (73-29), g: chalcopyrite in a matrix of pyrite with fossil remnants of tubular organism, which is highlighted by a red box (73-29), h: chalcopyrite altered to chalcocite along micro-fractures (45-7C), i: covellite surrounding chalcopyrite (55-6A). Mineral abbreviations: Ccp: chalcopyrite, Cct: chalcocite, Cv: covellite, Id: idaite, Iso: isocubanite, Mrc: marcasite, Py: pyrite, Sp: sphalerite, Gth: goethite

Fig. 3 Selection of minerals reported in the Cu-Fe-S system after Vaughan and Craig (1978) in atomic percent (at.-%) and the composition of the copper sulfides investigated in this study. Abbreviations: bn (bornite), cc (chalcocite), cp (chalcopyrite), cv (covellite), di (digenite), dj (djurleite), id-I (idaite, Cu_5FeS_6), id-II (idaite, Cu_3FeS_4)

Fig. 4 LA-ICP-MS transect across a chalcopyrite grain of a chimney fragment from New Mound 3 (55-6A). a: photomicrograph of transect and spots of laser ablation ICP-MS analyses; b: transect of logarithmic scaled concentrations of selected elements

Fig. 5 Scanning electron microscope elemental EDS map of a fluid conduit section from a chimney fragment (55-1A) illustrating the major element distribution on the scale of several mm. Three chalcopyrite (Ccp) generations occur. Ccp1 is coarse grained, Ccp2 is massive and forms the outer layer of the orifice. Ccp3 lines the inner l wall of the orifice. Other minerals present are idaite (Id), goethite (Gth) and marcasite (Mrc)

Fig. 6 Semi logarithmic scale histograms illustrating the variation in concentrations of selected elements in chalcopyrite from different chimney fragments of two sulfide mounds

Fig. 7 Box and whisker plots of selected trace element concentrations in chalcopyrite (n = 279) of different inactive sulfide mounds from the TAG hydrothermal field. Boxes show the upper and lower quartiles; the line between the boxes represents the median with the line bars indicating the variability outside the quartiles and the stars indicate minimum (*) and maximum (*) outliers. Chimney fragments: 55-6A (New Mound 3, n= 33) and 55-1A-Ccp3 (New Mound 2, n= 7) are plotted as representative samples for a high and low temperature composition; Southern mound: 21-3B (n=21), 50-14 (6.68 mbsf, n =39); Rona mound: 45-7C (n=25), 65-9 (10.53 mbsf, n=33), 65-13 (11.40 mbsf, n=32), 65-23 (12.37 mbsf, n=28); MIR Zone: 73-18 (4.35 mbsf, n=32), 73-29 (7.04 mbsf, n=29)

643 **Fig. 8** Box and whisker plots of selected trace element concentrations (n = 36) in copper minerals others than chalcopyrite
644 of different inactive sulfide mounds from the TAG hydrothermal field. Boxes show the upper and lower quartiles; the line
645 between the boxes represents the median with the line bars indicating the variability outside the quartiles and the stars
646 indicate minimum (∗) and maximum (∗) outliers. Covellite: 21-3B_cv (n=6), 55-6A_cv (n= 2); chalcocite: 45-7C_cct
647 (n=11); idaite: 55-1A_id (n= 17)
648
649 **Fig. 9** Log-log plots of LA-ICP-MS trace metal concentrations in chalcopyrite showing relationships and correlations
650 between selected elements
651
652 **Fig. 10** Concentrations of selected trace elements in chalcopyrite and their associated secondary alteration copper mineral
653 from New Mound 2, 55-1A, (a), Rona mound (b), Southern mound (c) and New Mound 3, 55-6A (d)
654
655 **Fig. 11** Primitive mantle normalised metal pattern for chalcopyrite from different hydrothermally inactive sulfide mounds
656 from the TAG hydrothermal field. All mean trace metals concentrations were normalised to primitive mantle values from
657 Palme and O'Neill (2014)

Table

Sample ID	Characteristics	Location	Latitude	Longitude	Depth	Sampling	Ccp	Iso	Id	Cct	Cv	Py	Mrc	Sp	Others
JC138-021-3B	Massive sulfide	Southern Mound	26°09.35'N	44°49.02'W	3550	HyBIS	+	--	--	--	x	+++	--	o	+
JC138-050-14	Massive sulfide	Southern Mound	26°09.34'N	44°48.97'W	3541	RD2	+	--	--	--	--	+++	--	o	+
JC138-045-7C	sulfide breccia	Rona Mound	26°09.36'N	44°48.82'W	3535	HyBIS	++	--	--	+	o	++	x	o	x
JC138-065-9	Massive sulfide	Rona Mound	26°09.37'N	44°48.80'W	3541	RD2	x	--	--	--	--	+++	--	o	+
JC138-065-13	Massive sulfide	Rona Mound	26°09.37'N	44°48.80'W	3541	RD2	+	--	--	--	--	+++	--	o	x
JC138-065-23	Massive sulfide	Rona Mound	26°09.37'N	44°48.80'W	3542	RD2	+	--	--	--	--	+++	--	o	x
JC138-055-1A	Chimney	New Mound 2	26°09.51'N	44°49.17'W	3589	HyBIS	+++	--	+	--	+	++	+	x	+
JC138-055-6A	Chimney	New Mound 3	26°09.56'N	44°49.19'W	3598	HyBIS	++	x	--	--	x	+	++	x	++
JC138-073-18	Sulfide breccia	MIR Zone	26°08.61'N	44°48.41'W	3440	RD2	++	--	--	--	--	++	--	--	x
JC138-073-29	Sulfide breccia	MIR Zone	26°08.61'N	44°48.41'W	3443	RD2	++	--	--	--	--	+++	--	o	x

Abbreviations: -- absent, o traces (≤1%), x minor (1-5%), + common (5-25%), ++ abundant (25-50%), +++ dominant (≥50%)
Ccp (chalcopyrite), Iso (iscocubanite), Id (idaite), Cct (chalcocite), Cv (covellite), Py (pyrite), Mrc (marcasite), Sp (sphalerite),
Others include holes, silicates, barite, jarosite, atacamite, iron-oxyhydroxides

Figure 1

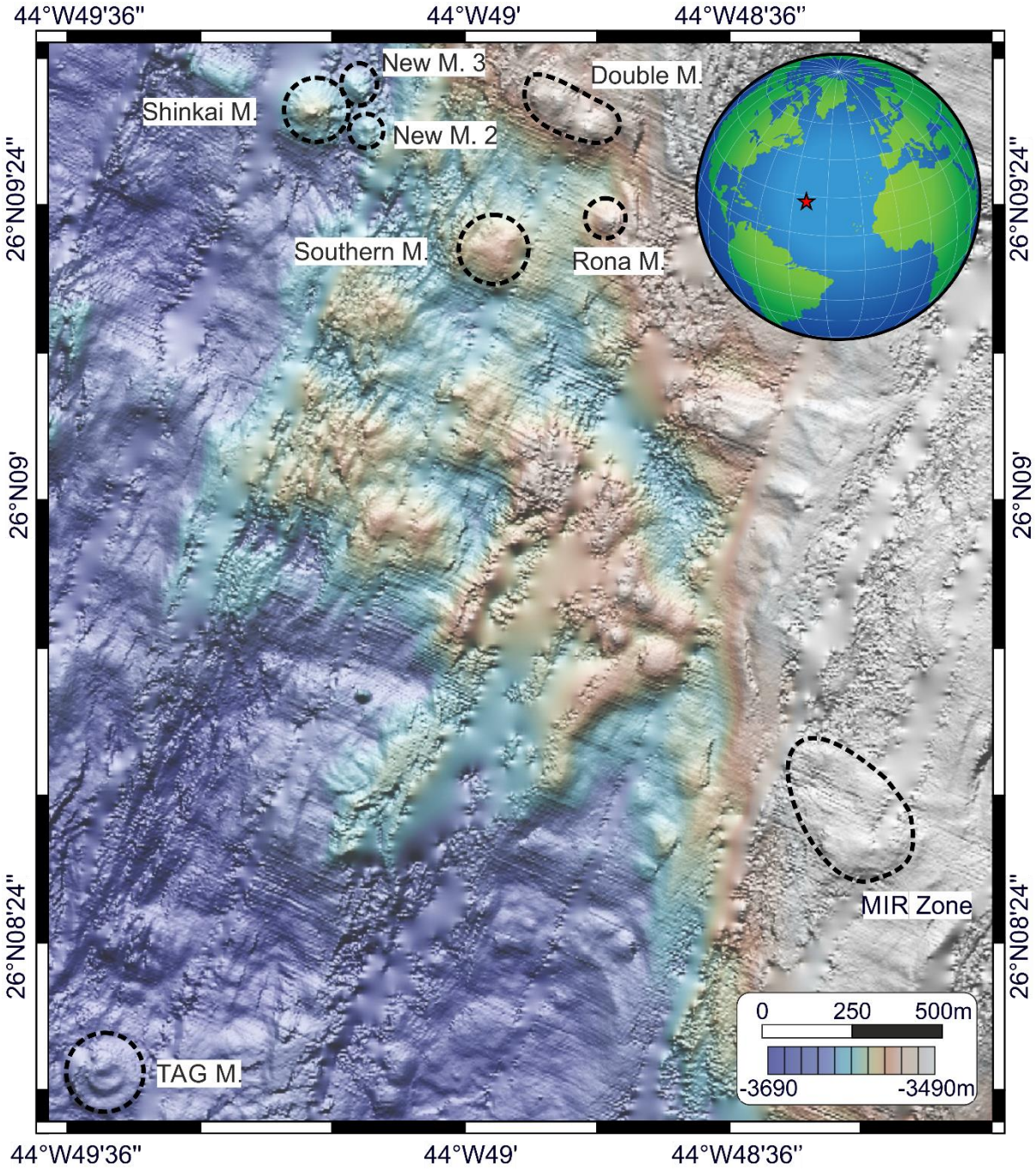
44°W49'36"
44°W49'
44°W48'36"
26°N09'24"
26°N09'
26°N08'24"
New M. 3
Double M.
Shinkai M.
New M. 2
Southern M.
Rona M.
MIR Zone
TAG M.
0
250
500m
-3690
-3490m

Figure 2

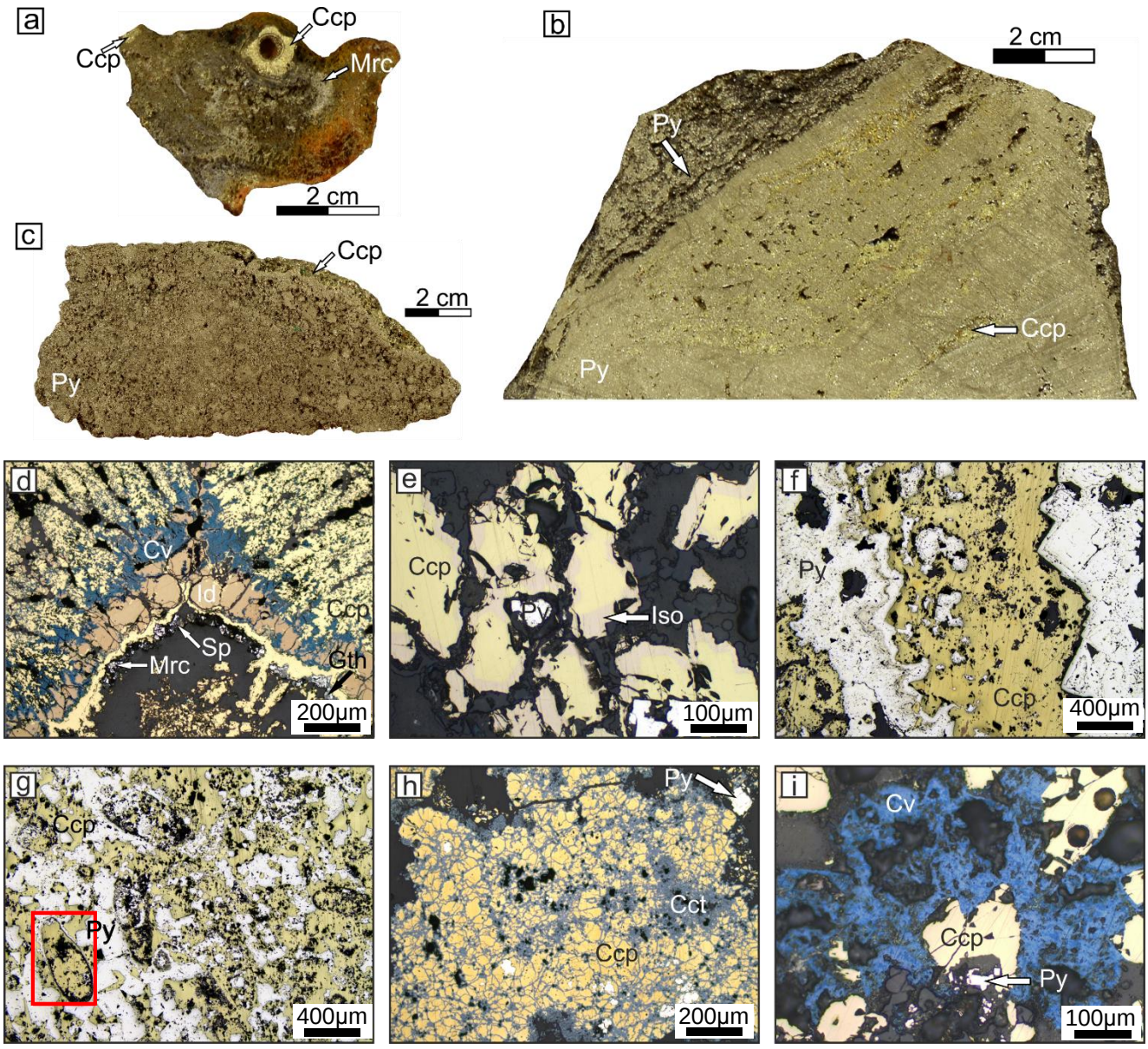
a
Ccp
Ccp
Mrc
2 cm
b
2 cm
Py
Ccp
Py
c
Ccp
2 cm
Py
d
Cv
Id
Ccp
Sp
Mrc
Gth
200μm
e
Ccp
Py
Iso
100μm
f
Py
Ccp
400μm
g
Ccp
Py
400μm
h
Py
Cct
Ccp
200μm
i
Cv
Ccp
Py
100μm

Figure 3

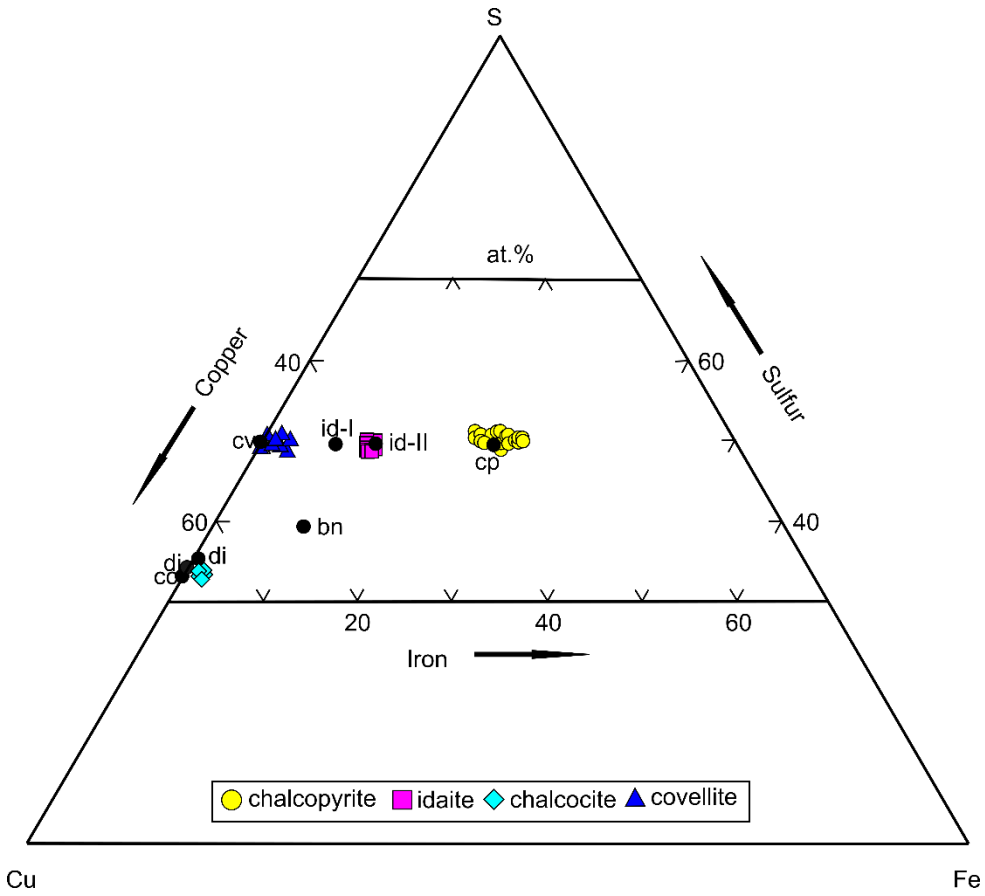
S
at.%
Copper
Sulfur
40
60
60
40
20
40
60
Iron
Cu
Fe
cv
id-I
id-II
cp
bn
di
di
co
chalcopyrite
idaite
chalcocite
covellite

Figure 4

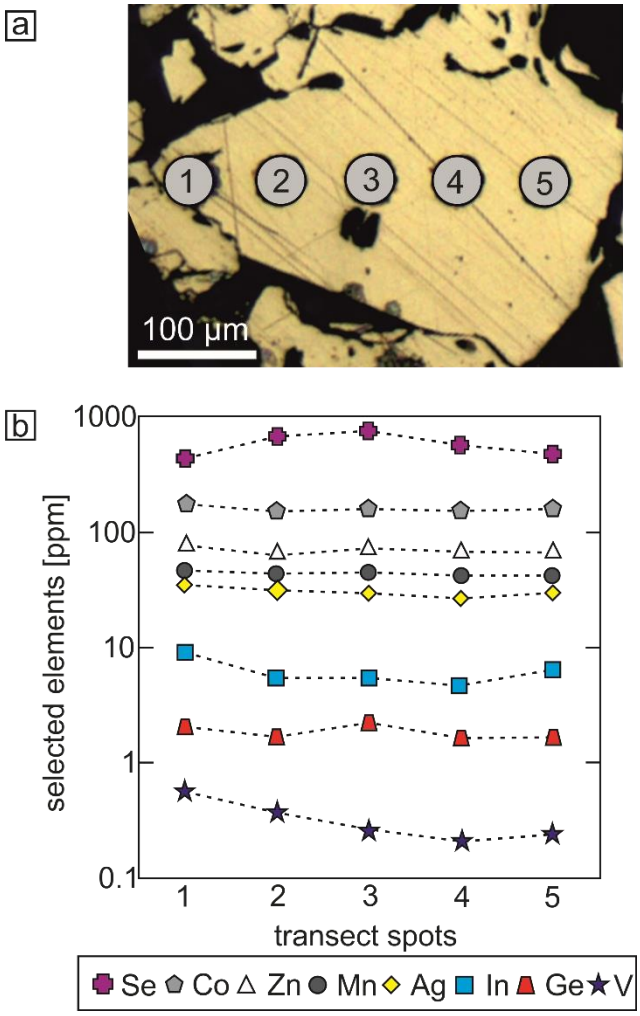
a
1
2
3
4
5
100 µm
b
1000
100
10
1
0.1
selected elements [ppm]
1
2
3
4
5
transect spots
Se Co Zn Mn Ag In Ge V

Figure 5

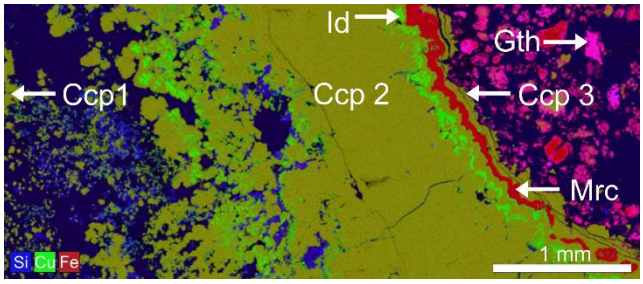

Figure 6

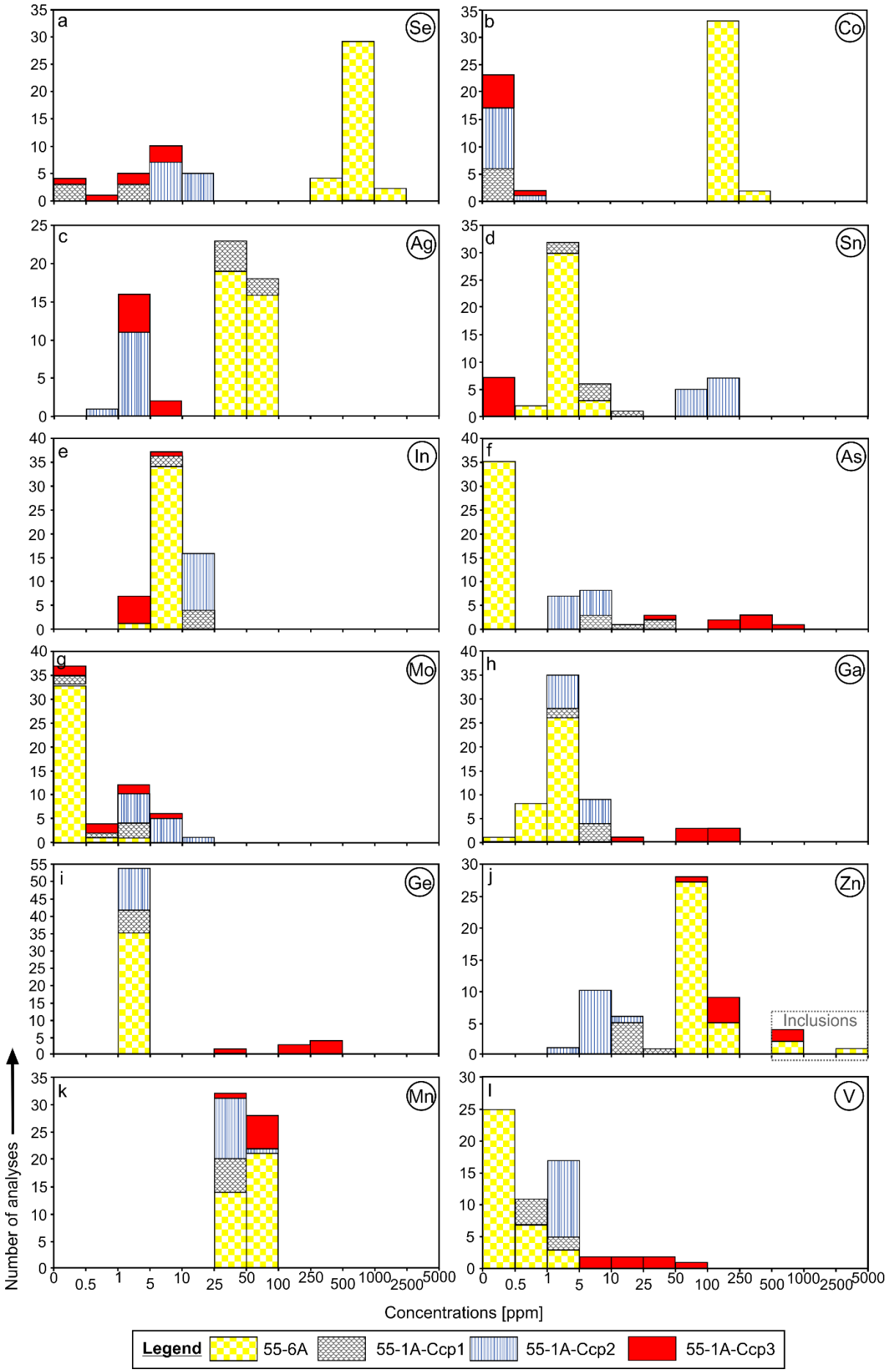
a
Se
b
Co
c
Ag
d
Sn
e
In
f
As
g
Mo
h
Ga
i
Ge
j
Zn
Inclusions
k
Mn
l
V
Number of analyses
0 0.5 1 5 10 25 50 100 250 500 1000 2500 5000
Concentrations [ppm]
Legend
55-6A
55-1A-Ccp1
55-1A-Ccp2
55-1A-Ccp3

Figure 7

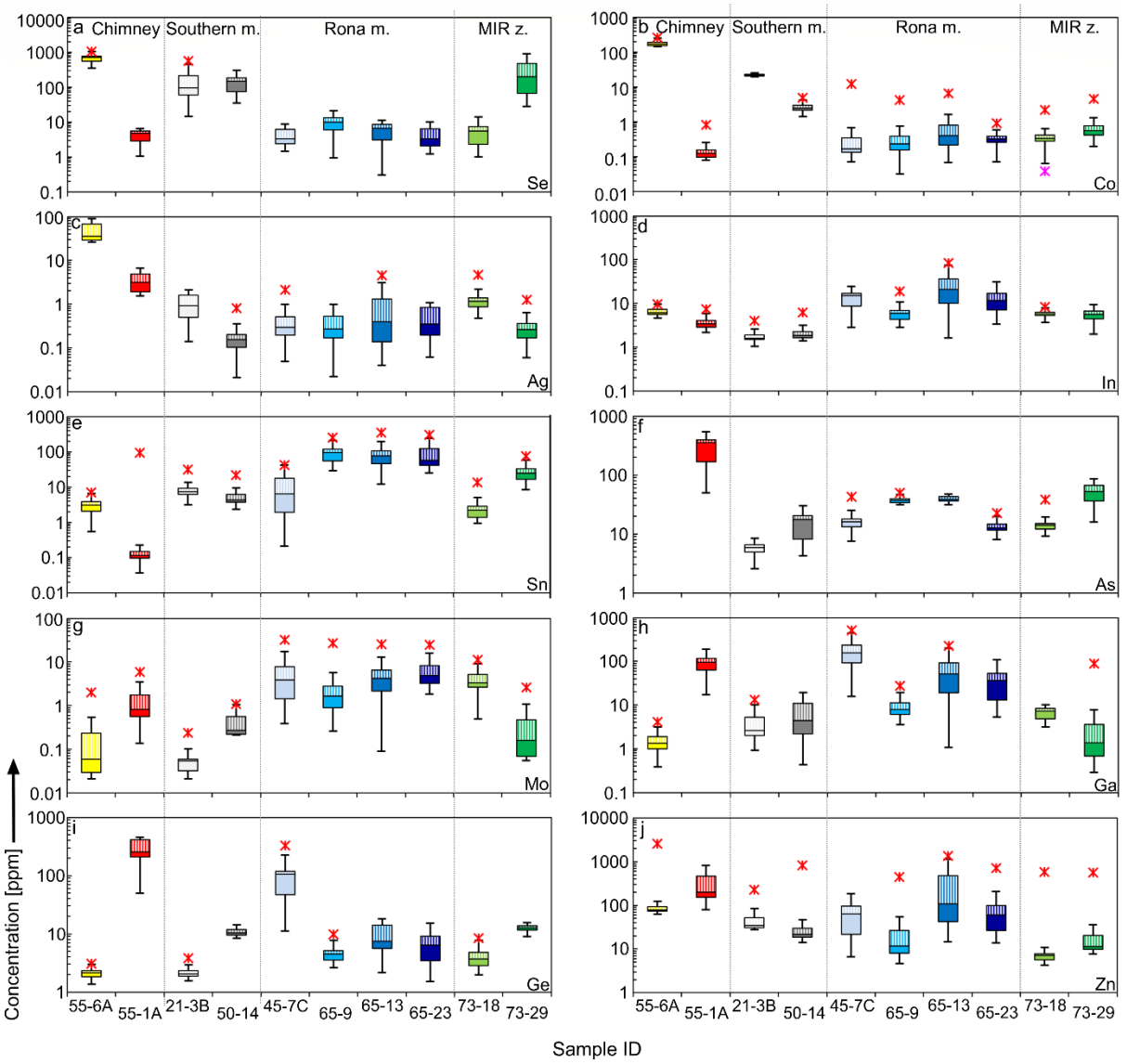
a Chimney
Southern m.
Rona m.
MIR z.
Se
b Chimney
Southern m.
Rona m.
MIR z.
Co
c
Ag
d
In
e
Sn
f
As
g
Mo
h
Ga
i
Ge
j
Zn
Concentration [ppm]
55-6A
55-1A
21-3B
50-14
45-7C
65-9
65-13
65-23
73-18
73-29
Sample ID

Figure 8

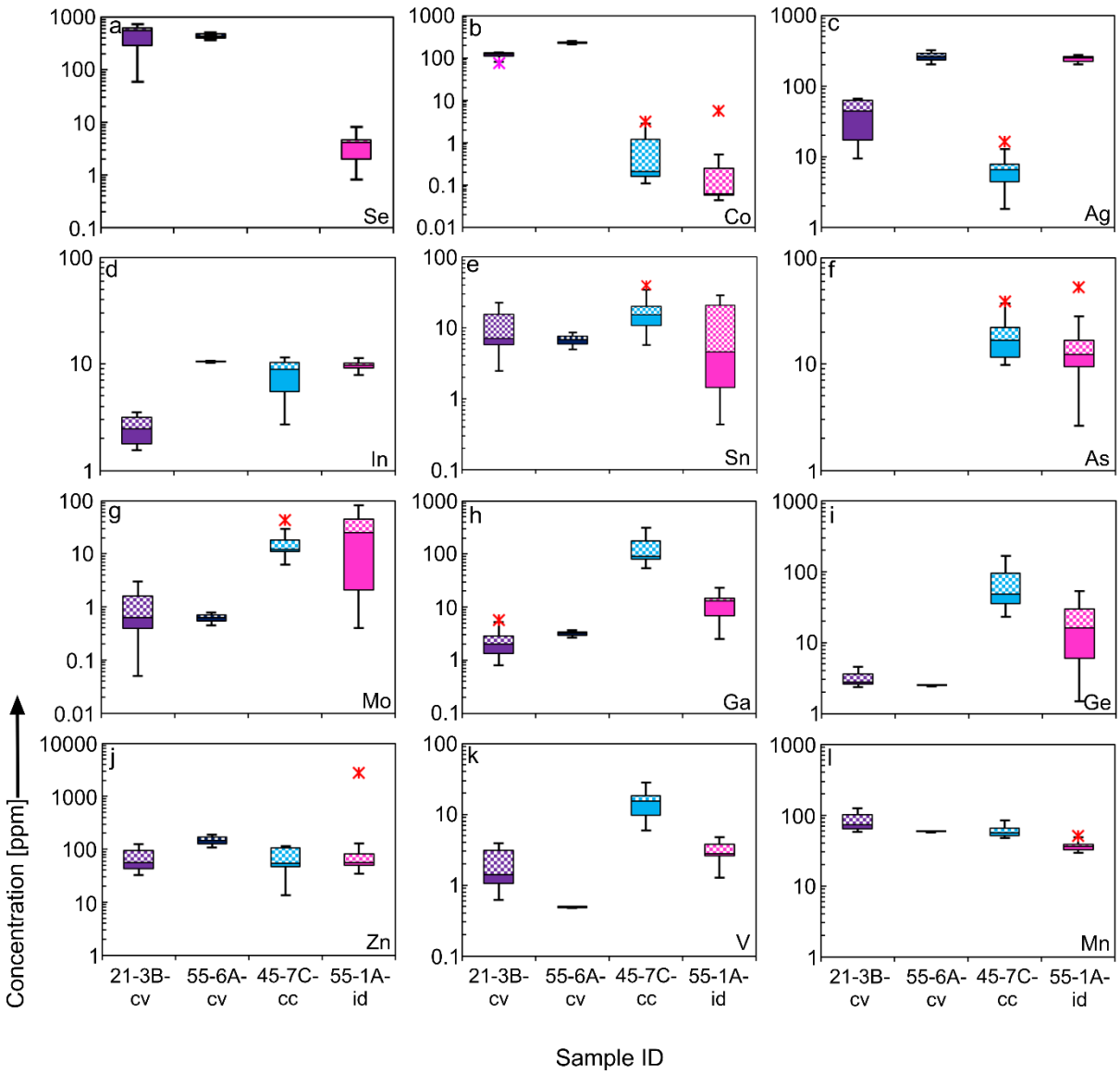
a
Se
b
Co
c
Ag
d
In
e
Sn
f
As
g
Mo
h
Ga
i
Ge
j
Zn
k
V
l
Mn
Concentration [ppm]
21-3B-cv
55-6A-cv
45-7C-cc
55-1A-id
Sample ID

Figure 9

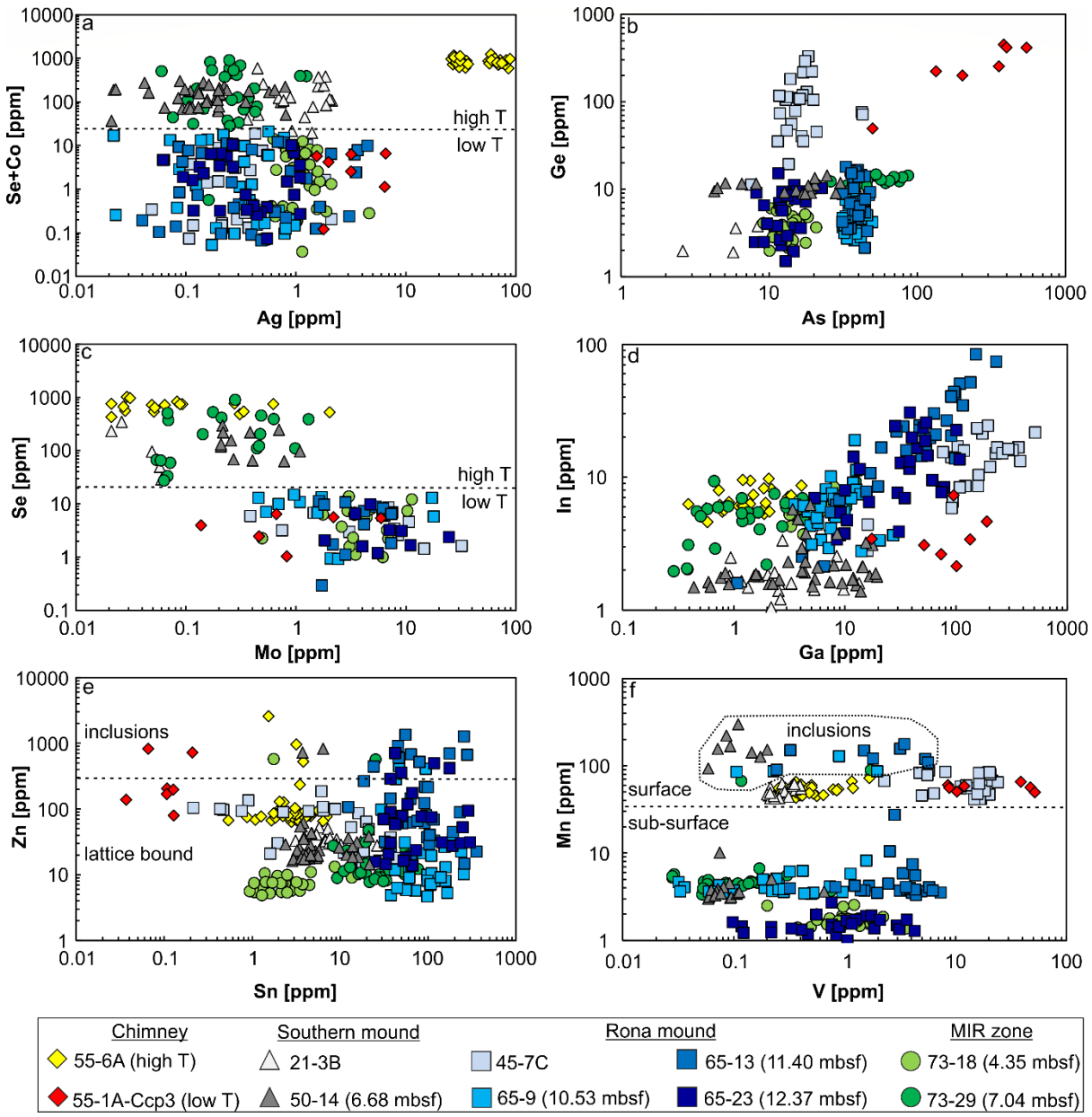
a
Se+Co [ppm]
Ag [ppm]
high T
low T
b
Ge [ppm]
As [ppm]
c
Se [ppm]
Mo [ppm]
high T
low T
d
In [ppm]
Ga [ppm]
e
Zn [ppm]
Sn [ppm]
inclusions
lattice bound
f
Mn [ppm]
V [ppm]
inclusions
surface
sub-surface
Chimney
55-6A (high T)
55-1A-Ccp3 (low T)
Southern mound
21-3B
50-14 (6.68 mbsf)
Rona mound
45-7C
65-9 (10.53 mbsf)
65-13 (11.40 mbsf)
65-23 (12.37 mbsf)
MIR zone
73-18 (4.35 mbsf)
73-29 (7.04 mbsf)

Figure 10

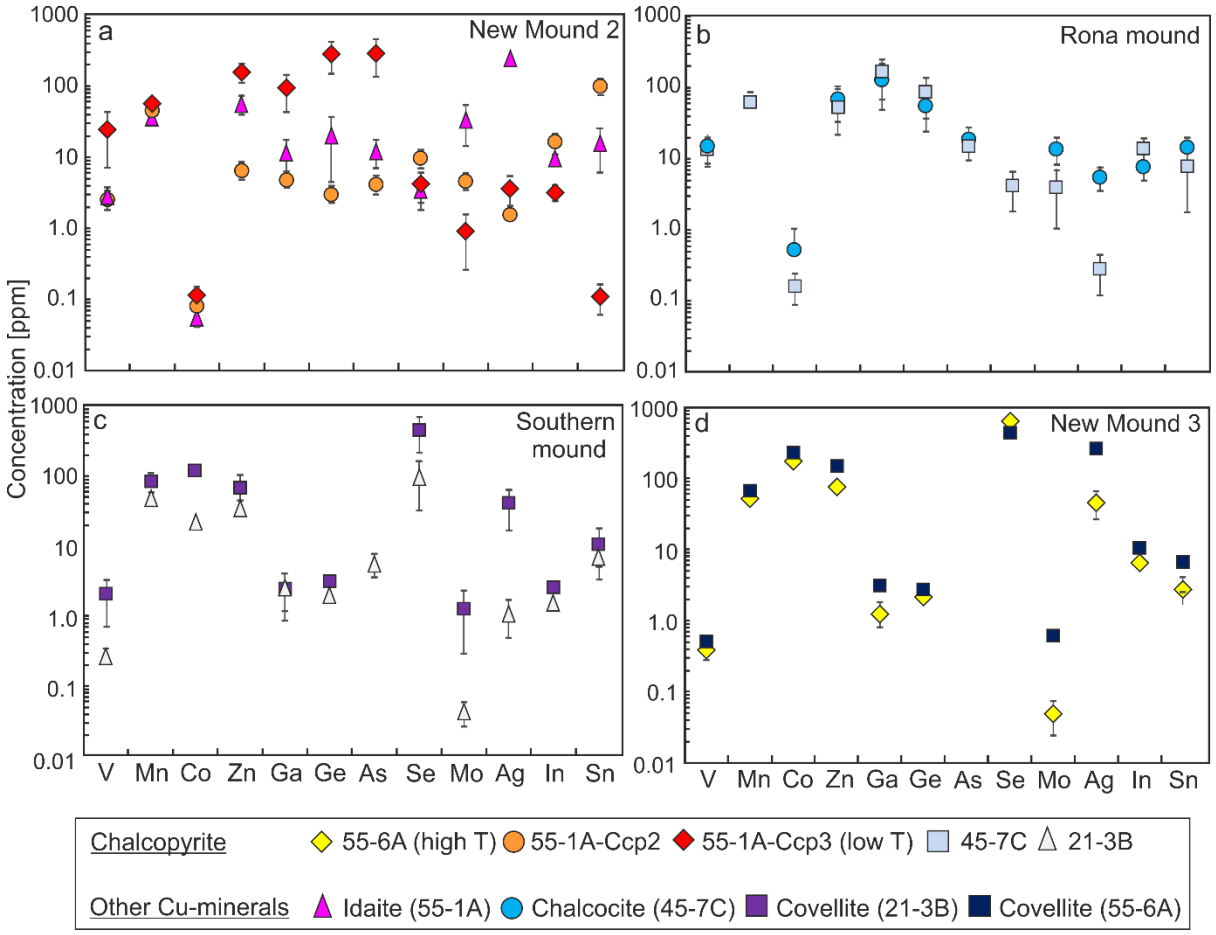
a
New Mound 2
b
Rona mound
c
Southern mound
d
New Mound 3
Concentration [ppm]
1000
100
10
1.0
0.1
0.01
V Mn Co Zn Ga Ge As Se Mo Ag In Sn
Chalcopyrite
55-6A (high T)
55-1A-Ccp2
55-1A-Ccp3 (low T)
45-7C
21-3B
Other Cu-minerals
Idaite (55-1A)
Chalcocite (45-7C)
Covellite (21-3B)
Covellite (55-6A)

Figure 11

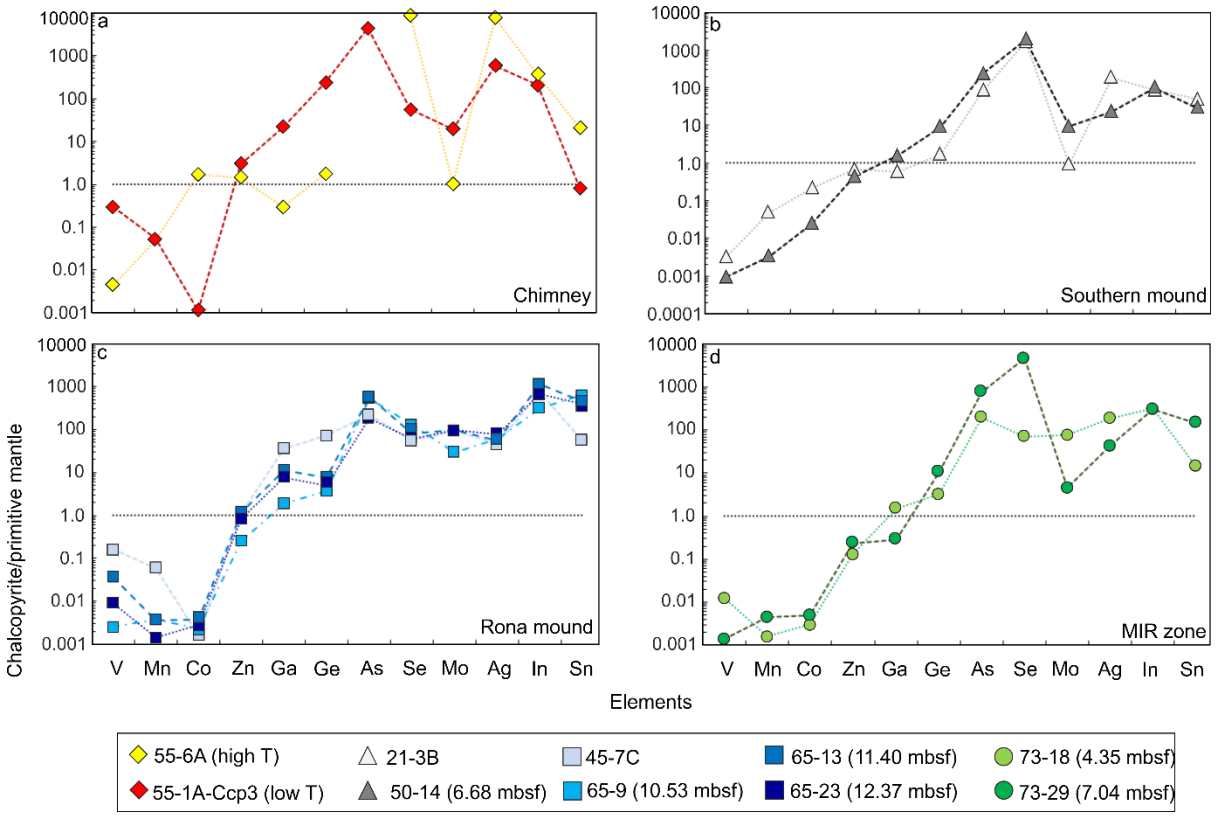
a
Chimney
b
Southern mound
c
Rona mound
d
MIR zone
Chalcopyrite/primitive mantle
V Mn Co Zn Ga Ge As Se Mo Ag In Sn
Elements
55-6A (high T)
55-1A-Ccp3 (low T)
21-3B
50-14 (6.68 mbsf)
45-7C
65-9 (10.53 mbsf)
65-13 (11.40 mbsf)
65-23 (12.37 mbsf)
73-18 (4.35 mbsf)
73-29 (7.04 mbsf)

Click here to access/download

Supplementary Material

ESM1.xlsx